Dielectronic recombination of W^{20+} ($4d^{10}4f^8$): Addressing the half-open f shell

N. R. Badnell,[1,*] C. P. Ballance,[2] D. C. Griffin,[3] and M. O'Mullane[1]

[1]*Department of Physics, University of Strathclyde, Glasgow G4 0NG, United Kingdom*

[2]*Department of Physics, Auburn University, Auburn, Alabama 36849, USA*

[3]*Department of Physics, Rollins College, Winter Park, Florida 32789, USA*

(Received 9 April 2012; published 29 May 2012)

A recent measurement of the dielectronic recombination (DR) of W^{20+} [Schippers *et al.*, Phys. Rev. A **83**, 012711 (2011)] found an exceptionally large contribution from near-threshold resonances ($\lesssim$1 eV). This still affected the Maxwellian rate coefficient at much higher temperatures. The experimental result was found to be higher by a factor of 4 or more than that currently in use in the 100- to 300-eV range, which is of relevance for modeling magnetic fusion plasmas. We have carried out DR calculations with AUTOSTRUCTURE which include all significant single-electron promotions. Our intermediate-coupling (IC) results are more than a factor of 4 larger than our LS-coupling ones at 1 eV but still lie a factor of 3 below experiment here. If we assume complete (chaotic) mixing of near-threshold autoionizing states, then our results come into agreement (to within 20%) with experiment below $\lesssim$2 eV. Our total IC Maxwellian rate coefficients are 50%–30% smaller than those based on experiment over 100–300 eV.

DOI: 10.1103/PhysRevA.85.052716 PACS number(s): 34.80.Lx, 34.80.Dp

I. INTRODUCTION

Tungsten will be a key element [1] in the ITER magnetic fusion device [2–4] currently under construction at Cadarache in France [5]. Its ability to withstand high power loads means that it will be the primary facing material within the vacuum vessel. Its high nuclear charge means also that it is potentially a serious contaminant in the sense of its ability to quench the fusion reaction due to radiative power loss. Intensive studies are under way at all of the world's major magnetic fusion laboratories to understand, predict, and control its behavior. The recent ITER-like wall upgrade at JET [6] provides the closest reactor environment short of ITER itself. The 74 ionization stages of tungsten may seem daunting from the detailed theoretical perspective. Reality is somewhat different. Very few ionization stages are observed in practice. Near neutrals are seen as they sputter off surfaces. Then many ionization stages burn through quite rapidly before ions of a much higher charge state are observed in particular localized environments. W^{20+} is a significant stage for spectral diagnostics and is seen at the null point of the separatrix at JET. W^{44+} performs a similar function at the core and is observed by the JET KX1 spectrometer. The ionization stages will change with the much larger and hotter ITER device but the principle remains the same: very few stages need to be modeled in detail. The great bulk of them can be modeled more "coarsely" as superstages. Detailed studies are being made of these key stages. One of the most basic and important theoretical quantities is the tungsten ionization balance since it is the main determinant of the intensity of spectral line emission. Electron-collisional equilibrium is a balance between electron-impact ionization and dielectronic recombination (DR). (All other recombination processes are negligible in the magnetic fusion domain.) A sufficiently accurate theoretical description of DR is key.

A recent experiment on W^{20+} ions by Schippers *et al.* [7] at the TSR storage ring in Heidelberg measured an exceptionally large DR merged-beam "rate coefficient" at a few electron volts: so much so that its contribution at the temperatures of significant fractional abundance for W^{20+} (100–300 eV) gave rise to a Maxwellian rate coefficient that is a factor of 4 or more higher than that currently used by the main magnetic fusion modeling package: the Atomic Data and Analysis Structure (ADAS) [9]. We seek to resolve this discrepancy.

There is little previous detailed work on DR for f-shell ions. At one end ($4d^{10}4f$) there are calculations for Gd^{17+} by Dong *et al.* [10] utilizing the Flexible Atomic Code (FAC) [11] which are relevant for modeling soft x-ray lithography. At the other end ($4d^{10}4f^{13+}$) there are calculations for Au^{20+} by Ballance *et al.* [12] with AUTOSTRUCTURE [13]. The results of Ballance *et al.* are in good agreement with the measurements of Schippers *et al.* [8] from 2 meV up to 10 eV. Both of the above approaches are standard level-resolved calculations which allow for single-electron promotions plus capture. They are largely restricted to, at most, doubly excited configurations and interactions thereof.

The recombination of open f-shell ions likely involves multi-excited-electron resonances [14,15]. Previous calculations on such ions are apparently limited to the configuration average (CA) approximation, the Burgess General Program (BBGP) [16,17], and others of that ilk, which are the mainstay of modeling codes. The calculations of Flambaum *et al.* [15] for the recombination of Au^{25+} (which is isoelectronic with W^{20+}) can be viewed as a form of partitioned CA. They utilize expressions for the radiative rate and autoionization rate which are similar to those of the CA. The near-threshold autoionization rates are partitioned over a Breit–Wigner distribution which is characterized by a single spreading width [14]. This compares with our previous CA work [18], which partitions them over the nonmetastable core levels according to their statistical weight. Such a partitioning maintains the allowed- vs forbidden-channel nature which is characteristic of DR in simple systems. The justification of the Breit–Wigner

*badnell@phys.strath.ac.uk

form and the spreading width follows from the complexity of the open f-shell ions in which configuration mixing tends to a chaotic limit which can be described by statistical theory [19]. This leads to a structureless continuum for the near-threshold merged-beams "DR" rate coefficient. The Au^{25+} results of Flambaum *et al.* [15] were found to be in good agreement with the measurements of Hoffknecht *et al.* [20] below 1 eV.

The approach to DR reported on in this paper is a detailed (level-to-level) one with single-electron promotions plus capture for all significant contributing configurations. The configuration mixing (and spin-orbit mixing) that we allow for is the same as done in our previous work on open Fe M-shell ($3p^q$) [21] and open Sn N-shell ($4d^q$) [22] ions. This allows for the mixing of all autoionizing configurations within the $(N+1)$-electron complex when the promoted and captured electrons have the same principal quantum number. The inequivalent case restricts the mixing to configurations of the N-electron core, i.e., with common Rydberg nl quantum numbers. This approach gives rise to a near-structureless continuum for the near-threshold merged-beams DR rate coefficient for these Fe and Sn cases. We seek to extend this work to the half-open f shell and to compare the near-threshold merged-beams DR rate coefficient with the measurements by Schippers *et al.* [7]. We seek also to determine the high-energy Maxwellian DR rate coefficient applicable to the diagnostic modeling of W^{20+} in magnetic fusion plasmas.

We provide a description of our background theory in Sec. II. We describe its application to W^{20+} in Sec. III. We present our results and compare them with those of experiment in Sec. IV. We make some concluding remarks in Sec. V.

II. THEORY

We use the independent processes and isolated resonance approximations to describe DR [16]. The oft-repeated working equations may be found in Ref. [21] along with a more expansive discourse on the methodology we employ. We summarize some pertinent points.

A. Methodology

We use the computer code AUTOSTRUCTURE [13] to calculate all relevant atomic parameters: energy levels, radiative rates, and autoionization rates. A multiconfiguration expansion is used in an LS-coupling or intermediate-coupling (IC) representation. The CA representation [23,24] is a simpler approach which is very useful for complex heavy species since it provides a rapid overview of the problem.

All of our previous work with the CA approximation utilized the DRACULA code [24,25]. One immediately sees the effect of level resolution and fine-structure mixing when comparing LS-coupling with IC results obtained with AUTOSTRUCTURE. Comparison of LS coupling with CA results has been clouded by the fact that DRACULA is based on the Cowan structure code [26]. The Cowan code utilizes κ-averaged Hartree-Fock radial orbitals [27]. The differences here vs AUTOSTRUCTURE can be minimized by its use of κ-averaged orbitals computed in self-consistent CA model potentials [26]. The Cowan code generally also scales various operator interactions.[1] This facility is not readily or generally available in AUTOSTRUCTURE. We have implemented the CA angular momentum representation within AUTOSTRUCTURE. This eliminates any uncertainty in seeing the pure effect of moving to a configuration-mixed term-resolved representation. We have carried out detailed CA comparisons between AUTOSTRUCTURE and DRACULA in the course of the present work so as to verify the integrity of the new development.

B. Computation

The (near-) half-open f-shell problem is a daunting one. If we view it simply in terms of binomial coefficients for the number of states present in a configuration, then moving from the $4d^{10}4f^{13}$ ground configuration considered in Ref. [12] to $4d^{10}4f^8$ increases the number of states by a factor of (429/2). Memory requirements (CPU and disk) scale as $(429/2)^2$, and the time requirement as $(429/2)^3$. This is all relative. Absolute numbers are much larger once we start promoting electrons from the $4d$ and $4f$ subshells of the ground configuration. (The only bonus of the binomial effect is that $4f^7$ is only marginally worse than $4f^8$ since the number of states increases only by a factor 8/7.)

The published AUTOSTRUCTURE code [13] was used for our recent work on the tin half-open d shell [22] and $Au^{20+}4f^{13}$ [12]. It does not scale to the half-open f shell. Substantial development has been necessary. A detailed exposition is more suited to a computer physics journal, and so we give only a flavor here.

Most angular momentum packages used by atomic structure and collision codes are based on Racah algebra. This is a hierarchical coupling scheme. A complication for the open f shell is the need to introduce a new quantum number: seniority. AUTOSTRUCTURE employs the nonhierarchical Slater-state approach to angular momentum coupling that was advocated by Condon and Shortley [28]. It has no concept of parentage.[2] All interactions are expanded and determined initially in an uncoupled (Slater-state) representation. A transformation is then made to an LS and/or LSJ representation through the use of vector-coupling coefficients (VCCs). The half-open f shell requires billions of coefficients and so tens of gigabytes of RAM per processor. They are not all required at the same time. It has been possible to implement an archive on disk in a way that does not swamp the calculation with I/O.

Another issue concerns the large number of radiative and autoionization rates that arise in a level-resolved calculation. The approach to date has been to archive them all to disk for subsequent processing in a variety of ways: to compare with experiment, or to generate total rate coefficients for astrophysical modeling, or to process as final-state resolved data for collisional-radiative modeling for magnetic fusion. Such general flexibility comes at the cost of many terabytes of disk space and corresponding I/O time. If we sacrifice some degree of generality, then we can carry out bundling over quantum numbers and summation of partial widths on the fly

[1] It does not do so under CA operation.

[2] It is both possible and advantageous to introduce some parentage, but it is not required.

as the atomic data are generated. This reduces the data files to a manageable size. The user choice of bundling and/or summation should be guided by the exact same implementation made within the collisional-radiative modeling approach so as to render it tractable for heavy species. It is important to note that this introduces *no* additional approximation for our description of the experimental DR cross section or the total Maxwellian rate coefficients presented later.

We do not dwell on various RAM and CPU time issues that arose as well on scaling from the open d to the f shell. It is sufficient to note that the calculations reported on below took about 2 weeks on a modest cluster (the problem does not engender large-scale parallelization) with 4 Gb RAM and 250 Gb of scratch disk per processor.

C. Mixing

We discuss the role of (configuration) mixing of autoionizing states on DR in complex heavy species. This is important since we include only a limited amount (see the next section). We note that we use the term DR to describe all resonant recombination mediated by a two-body operator and products thereof. We do not subcategorize into higher order contributions those processes which arise from the same configuration-mixed procedure, *viz.,* trielectronic recombination, etc.

We consider a model problem in which we include only autoionizing configurations which result from single-electron promotions plus capture from the ground configuration. We assume that the autoionization rates (A_1) and radiative rates (R) satisfy $A_1 \gg R$. Then the DR cross section is basically proportional to R for a fixed symmetry. (We consider only autoionizations which are inverses of the dielectronic capture in this model, i.e., near-threshold.) Now consider the addition of autoionizing configurations which result from double-electron promotions plus capture from the ground configuration. This set is only populated by mixing with the first via a unitary transformation. We denote the second set of autoionization rates A_2 and assume similar radiative rates (R). We assume $A_2 \ll R$. If mixing between the two sets is strong enough and there are enough states, then the autoionization rates for the first set (which we now label A_{12}) are depleted to the extent that $A_{12} \ll R$. The DR cross section is now proportional to $A_{12} + A_2 = A_1$. The total is *enhanced* by a factor of A_1/R. (Mixing only takes place between states of the same statistical weight and so the sum over autoionizing states is assumed to be implicit.) We consider the effect of further mixing. Now add configurations which result from triple-electron promotions plus capture from the ground configuration. Denote the autoionization rates for the three sets A_{123}, A_{23}, and A_3. Assume all $A_i \ll R$ still. The total DR cross section is unchanged since it is still proportional to $A_{123} + A_{23} + A_3 = A_1$. Such mixing is merely *redistributive* and so can be neglected with respect to the total DR.

This is the nature of the near-threshold DR problem in complex ions described by Flambaum *et al.* [15] (for Au^{25+}) following a preliminary earlier study [14]. The chaotic fully mixed nature of Au^{24+} was verified by Gribakin and Sahoo [29], who performed large-scale calculations of eigenenergies and eigenvectors. Our detailed description of the autoionizing spectrum is necessarily incomplete. The above discussion is intended to shed light on how far we need to go. The model problem was merely illustrative in using configuration mixing via different sets of promotions. We are largely restricted to one-electron promotions plus capture since we need to compute autoionization rates and radiative rates which are applicable over a much wider range of energies. But we do have differing representations: CA, LS coupling, and IC. The question, then, is the degree to which the IC representation is incomplete with regard to enhancement or whether it has moved to a redistributive regime so that our DR cross sections will have converged largely with respect to the total. The structured behavior of our low-energy cross section and its comparison with experiment and with statistical theory will enable us to judge the degree to which this is so. (It is straightforward to apply the statistical approach to our data—we simply partition our autoionization rates using the Breit–Wigner distribution—but note that this procedure is only valid near threshold.)

III. APPLICATION

The ground configuration of W^{20+} is [Kr]$4d^{10}4f^8$. The ground term is ^7F. The ground level is $J = 6$. These denote the ground state of the CA, LS-coupling, and IC representations. We describe the DR reactions that we take account of by their configuration representation. This consists of N-electron configurations to which a continuum electron and a Rydberg electron are each coupled. This describes dielectronic capture and/or autoionization. The latter describes radiative transitions within the core also. Additional $(N+1)$-electron "correlation" configurations are added to describe Rydberg electron radiation into the core. Rydberg-Rydberg radiation $n \to n' > 4$ is described hydrogenically. We break down the problem by target subshell promotion.

A. $\Delta n = 0$

We allow for $4d \to 4f$ and $4f \to 4f$ promotions in both LS coupling and IC. The latter promotion does not contribute to CA DR since it corresponds to an elastic transition. The N-electron configurations are $4d^{10}4f^8$ and $4d^9 4f^9$. The $(N+1)$-electron configurations are $4d^{10}4f^9$ and $4d^9 4f^{10}$. We note that some terms or levels of $4d^{10}4f^7 5l$ lie below $4d^9 4f^9$. The former could provide an alternative autoionization channel for the latter. Such a transition is forbidden directly since it is described by a two-body operator. (A continuum electron is still to be coupled to the former, and a Rydberg to the latter.) It could take place via mixing if we were to include additional configurations. We do not. We also consider the $4p \to 4f$ promotion in CA only. Its contribution is expected to be small. We normally use the CA calculation to determine the range of Rydberg nl required to converge the total DR and then use these values for the more demanding LS-coupling and IC calculations. We find that the contribution to the Maxwellian rate coefficient from the $4d \to 4f$ promotion is converged to about 3% by $n = 100$ and $l = 7$ at all energies. It is not possible to do so for the $4f \to 4f$ promotion since the CA result is 0, and so we utilize the LS-coupling calculation here to delimit the IC one. We find that the contribution from the

$4f \to 4f$ promotion is converged to about 3% by $n = 100$ and $l = 6$ at all energies.

B. $\Delta n = 1$

We consider the $4d$ and $4f$ promotions separately.

1. $4f \to 5l$

The N-electron configurations are $4f^8$ and $4f^75l$ ($l = 0$–4). It is necessary to omit the $n = 5$ continuum so as to keep the problem tractable in the LS-coupling and IC calculations.[3] We carried out CA calculations both with and without the $n = 5$ continuum to aid our analysis of the uncertainty (overestimate) in our LS-coupling and IC results. There is none at all below ~20 eV since they are all energetically closed.

The $(N + 1)$-electron configurations are $4f^85l$ ($l = 0$–4). Some of the $4f^75l5l'$ configurations are (partially) bound. We treat such $n \to n' = 5$ radiation hydrogenically (approximately) in the LS-coupling and IC calculations. They are either strictly bound or autoionizing in the CA approximation. Their contribution is small.

The CA results for this promotion are converged to about 5% at 200 eV and 10% at 1000 eV upon summing to $l = 5$. The sum over n is converged to better than 2% by $n = 100$. We add this small "top-up" in l (and n, since we are doing so) from our CA results to the LS-coupling and IC ones.

2. $4d \to 5l$

The N-electron configurations are $4d^{10}4f^8$, $4d^94f^9$, $4d^94f^85l$ ($l = 0$–4) and $4d^{10}4f^75l$ ($l = 0$–4). We omit the $n = 5$ continuum again. The $4d^94f^8$ is rather demanding when coupled to $5lnl'$ for $l + l' > 5$. It has a factor of 70/8 more states than the corresponding $4d^{10}4f^7$. We need to consider it further. We write the dielectronic capture reaction in a somewhat unusual form:

$$4f^8(^7F)4d^{10} + e^- \to 4f^8(^7F)4d^95lnl'.$$

This illustrates the role of the $4f^8\,{}^7F$ ground term as a spectator. It cannot change simultaneously with the two-body dielectronic capture. It can change (shake up) via mixing in the autoionizing states. We omit such mixing. We do the same for the reverse radiative stabilization to $4f^8(^7F)4d^{10}nl$. This renders a tractable but reasonable description of the $4d \to 5l$ promotions. We recall that there is no configuration mixing whatsoever present in the CA approximation. We recall also the lack of sensitivity to configuration mixing that we found for total DR in the tin $4p - 4d$ transition array despite the demonstrable extensive configuration mixing [22]. Such an argument may not be valid near threshold; see the discussion in Sec. II C. We emphasize that we place no such restrictions (on mixing) when the $4f$ is active such as for the $4d^94f^9$ configuration. We have implemented the general user specification of term restrictions for spectator subshells within AUTOSTRUCTURE. These are common to all configurations which contain the specified subshell(s).

The $(N + 1)$-electron configurations are $4d^{10}4f^85l$ ($l =$ 0–4) and $4d^94f^95l$ ($l = 0$–4). A few of the $4d^94f^85l5l'$ configurations are (partially) bound and we treat them as for $4f \to 5l$.

The CA results for this promotion are converged to 1% at 1000 eV upon summing to $l = 4$. The sum over n is converged to much better than 1% by $n = 100$.

C. $\Delta n = 2$

We consider $4d + 4f \to 6l$ promotions within the CA approximation only. The contribution is expected to be small.

IV. RESULTS

We show an overview of the different CA contributions to the total DR Maxwellian rate coefficient in Fig. 1. The energy range of interest for an electron collisional plasma is 100–300 eV. This is where W^{20+} has its maximal fractional abundance (>0.01) in a magnetic fusion plasma.

We remark that the contribution from $4d \to 4f$ promotions is comparable with the $\Delta n = 1$ above ~100 eV. This is in contrast to the case of the almost-full $4f$ subshell of Au^{20+} [12]. It also dominates at a few electron volts, but this behavior can be expected to be more ion dependent.

We see that we do not need to consider $4p \to 4f$ and $\Delta n = 2$ promotions any further.

A. $\Delta n = 0$

We present and compare our LS-coupling and IC results for the $4f \to 4f$ and $4d \to 4f$ promotions in Fig. 2. We note

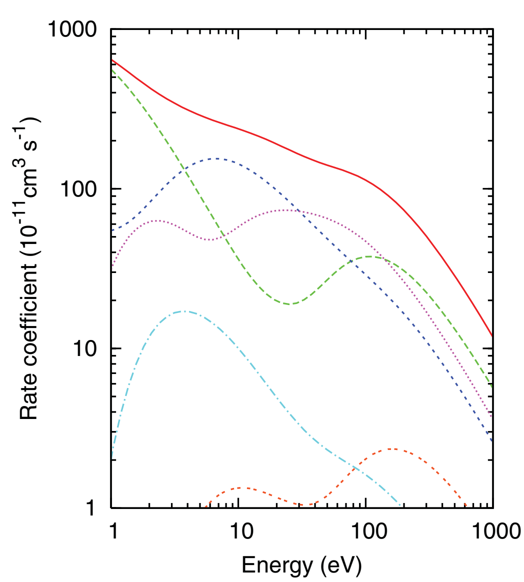

FIG. 1. (Color online) W^{20+} CA Maxwellian DR rate coefficient contributions for various promotions: total [solid (red) curve], $4d \to 4f$ [long-dashed (green) curve], $4f \to 5l$ [short-dashed (blue) curve], $4d \to 5l$ [dotted (magenta) curve], $4p \to 4f$ [dot-dashed (cyan) curve], and $4d + 4f \to 6l$ [double-dashed (orange) curve].

[3]The number of VCCs that need to be internally buffered becomes too large. A smaller buffer could be implemented but this would likely increase the I/O time substantially. The absolute number of VCCs required for LS-coupling is only typically a factor of 2 smaller than that for IC. The demands of the IC calculation arise from the fact that far more of the states that they represent interact.

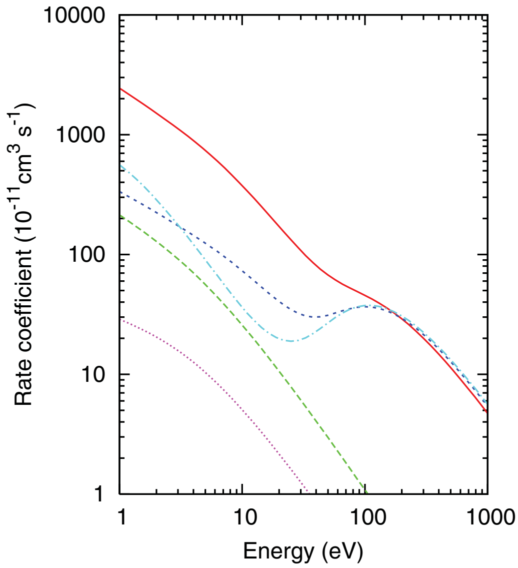

FIG. 2. (Color online) W^{20+} Maxwellian DR rate coefficient contributions for $\Delta n = 0$ promotions: IC $4d \to 4f$ [solid (red) curve], IC $4f \to 4f$ [long-dashed (green) curve], *LS* $4d \to 4f$ [short-dashed (blue) curve], *LS* $4f \to 4f$ [dotted (magenta) curve], and CA $4d \to 4f$ [dot-dashed (cyan) curve].

the close agreement between them and the CA results for the $4d \to 4f$ promotion above ~100 eV. There is about a factor of 7 difference between the *LS*-coupling and the IC results down to 1 eV. The contribution from the $4f \to 4f$ promotion is no more than about 10% that of the $4d \to 4f$ above 1 eV.

B. $\Delta n = 1$

1. $4f \to 5l$

We present and compare our *LS*-coupling and IC results for $4f \to 5l$ promotions in Fig. 3. We separate out the contributions from capture to $n = 5$ and $n > 5$. The sums of the two in *LS*-coupling and IC agree to within 10% by 100 eV. We show CA results both with and without autoionization to the $n = 5$ continuum. The rather pronounced high-energy peak is reduced by a factor of 2 at 160 eV. These are the first autoionizations into excited-state pathways in the CA-coupling scheme. The *LS*-coupling and IC are already suppressed by autoionization into (the continuum of) a multitude of excited states within the ground configuration. This is reflected in their less pronounced high-energy peaks. We would not expect the ($n > 5$) *LS*-coupling and IC results to be suppressed further by more than ~20% below 300 eV.

2. $4d \to 5l$

We present and compare our *LS*-coupling and IC results for $4d \to 5l$ promotions in Fig. 4. We see that the relative contributions from capture to $n = 5$ and $n > 5$ are reversed compared to the $4f \to 5l$ promotions. The $n > 5$ contribution does not exceed that of the $n = 5$ until high energies. This is due to autoionization suppression via the $4f \to 4d$ inner-shell transition. The CA results for $n > 5$ are suppressed by a factor of 2 at 160 eV, but the sum including $n = 5$, by about one-third. The ($n > 5$) *LS*-coupling and IC results are likely

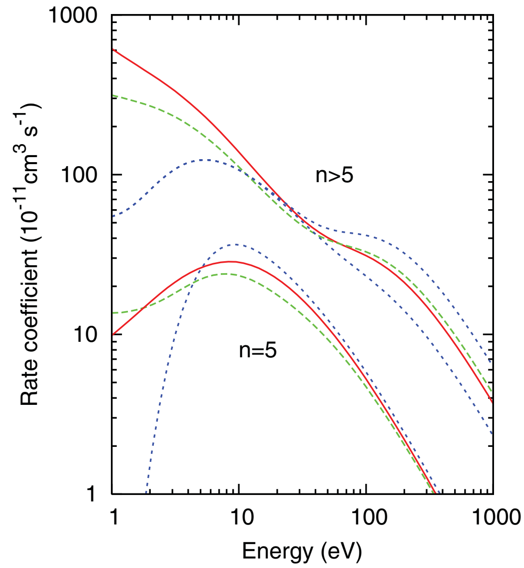

FIG. 3. (Color online) W^{20+} Maxwellian DR rate coefficient contributions for $4f \to 5l$ ($l = 0$–4) promotions (captures to $n = 5$ and $n > 5$ are shown separately): IC [solid (red) curves], *LS* [long-dashed (green) curves], and CA, $n > 5$ both with and without the $n = 5$ continuum [short-dashed (blue) curves].

to be suppressed by a larger relative factor than for the case of $4f \to 5l$ promotions, but the overall sum including $n = 5$ dilutes the factor and ~20% appears to be a reasonable estimate here.

C. Totals (merged beams)

We convoluted our DR cross sections with the electron velocity distribution applicable for merged electron-ion beams in the TSR cooler [7]. We compare our resultant total DR rate

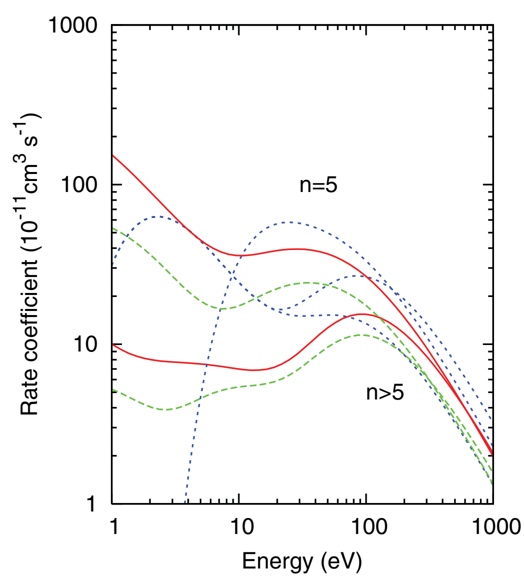

FIG. 4. (Color online) W^{20+} Maxwellian DR rate coefficient contributions for $4d \to 5l$ ($l = 0$–4) promotions (captures to $n = 5$ and $n > 5$ are shown separately): IC [solid (red) curves], *LS* [long-dashed (green) curves], and CA, $n > 5$ both with and without the $n = 5$ continuum [short-dashed (blue) curves].

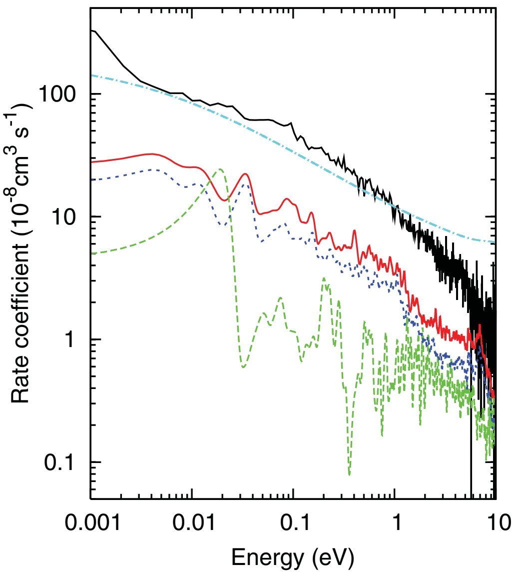

FIG. 5. (Color online) W^{20+} merged-beam DR rate coefficients: experiment [7] [upper solid (black) curve], partitioned total [dot-dashed (cyan) curve], IC total [lower solid (red) curve], *LS* total [long-dashed (green) curve], and IC $4d \rightarrow 4f$ only [short-dashed (blue) curve].

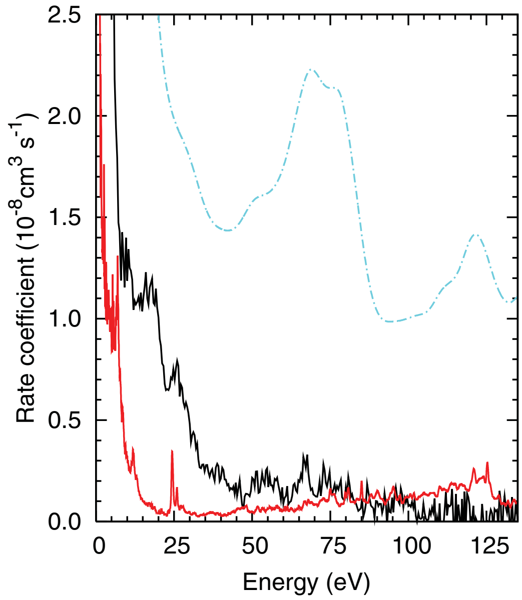

FIG. 6. (Color online) W^{20+} merged-beams DR rate coefficients: experiment [7] [rightmost solid (black) curve], partitioned total [dot-dashed (cyan) curve], and IC total [leftmost solid (red) curve].

coefficients with those measured on the TSR storage ring [7]. We focus first on the near-threshold region (0–10 eV) for which Schippers *et al.* reported the largest measured DR rate coefficient to date. Figure 5 shows that our IC results are larger by a factor of 2–5 than our *LS*-coupling results, but they are still typically a factor of 3 smaller than experiment. Our IC results are dominated by the $4d \rightarrow 4f$ promotion (80%). The density of resonances is such that there is little resultant structure in the total. We have a near-quasicontinuum of resonances. It does not matter, then, just where the ionization limit lies.

The remaining factor of ~3 is likely due to the incomplete mixing within our IC configuration expansion. We show results (Fig. 5) where we have partitioned our autoionization rates using the Breit–Wigner distribution with a spreading width of 10 eV [14]. The results are not particular sensitive to this width. Our CA, *LS*-coupling, and IC results are barely distinguishable on this scale and so we show a single curve. We obtain agreement with experiment to within 20% over 0.003–2 eV. Similar findings were obtained by Flambaum *et al.* [15] for Au^{25+}. (The measured cross section increases at energies below 0.003 eV due to an artifact of the merged-beam technique [30]).

The first excited level of the ground term opens up just below 2 eV. The experimental cross section falls away progressively thereafter (see Fig. 6). This fall off coincides with the opening-up of an increasing number of alternative autoionization channels. If autoionization into excited levels is fully redistributed as per the ground, then the total width is unaffected. The partitioned autoionization widths to the ground level are orders of magnitude smaller than the radiative widths. This is why the partitioned results are largely unchanged—even when summing over autoionization to hundreds of excited levels. In nature it appears that typical autoionizing widths to the ground level are no more than a factor of ~10 smaller than the radiative widths. Summing over a relatively small number of excited continua then produces a total autoionization width comparable to and then exceeding the radiative width. We note that our level-resolved autoionization widths typically are only larger than the radiative widths by, at most, a factor of 5–10. Experiment falls between the two theoretical "limits." The partitioned results are clearly inapplicable here.

All of our results are an upper limit because we assume 100% of the W^{20+} initial ion population to be residing in the ground state. Schippers *et al.* [7] identify several possible metastable levels that could remain populated during the lifetime of the measurement but have no estimate of their population. Any combination of metastables that we take reduces the total. This is because DR from excited states is suppressed by autoionization into the continuum attached to lower levels. Only the ground level is immune from this. The agreement between our Breit–Wigner partitioned results and experiment below 10 eV indicates that the metastable presence is not significant.

D. Totals (Maxwellian)

We turn now to the corresponding total Maxwellian DR rate coefficients. We compare results in Figs. 7 and 8. The two CA results (Fig. 7) illustrate the effect of the omission of $n = 5$ continuum suppression on the total. It is 25% at 160 eV. The lower CA, *LS*-coupling, and IC results are all in close agreement above ~100 eV. The *LS*-coupling and IC results are an upper limit not just because of the omission of the $n = 5$ continuum but also because they assume 100% of the W^{20+} initial ion population to be residing in the ground state.

The experiment by Schippers *et al.* [7] only detects resonances which occur below 140 eV. We show a second IC result (Fig. 8) which imposes such a cutoff. This cutoff result lies just over 50% below experiment at 160 eV. If

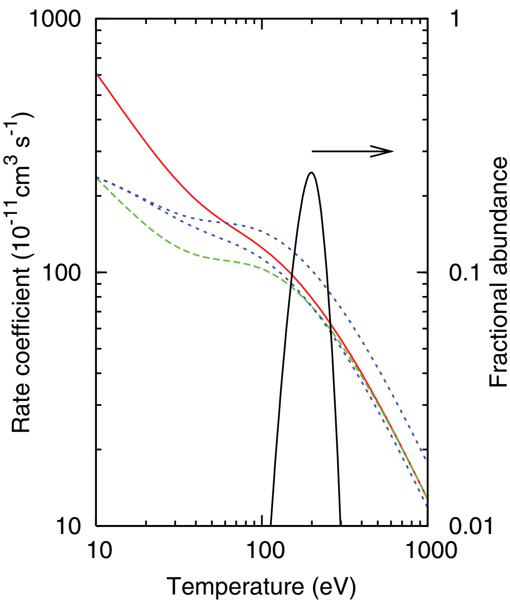

FIG. 7. (Color online) W^{20+} total Maxwellian DR rate coefficients: IC [solid (red) curve originating on y axis], *LS* [long-dashed (green) curve], and CA with and without the $n = 5$ continuum [short-dashed (blue) curves]. The fractional abundance of W^{20+} in a magnetic fusion plasma is also shown [solid (black) curve originating on x axis].

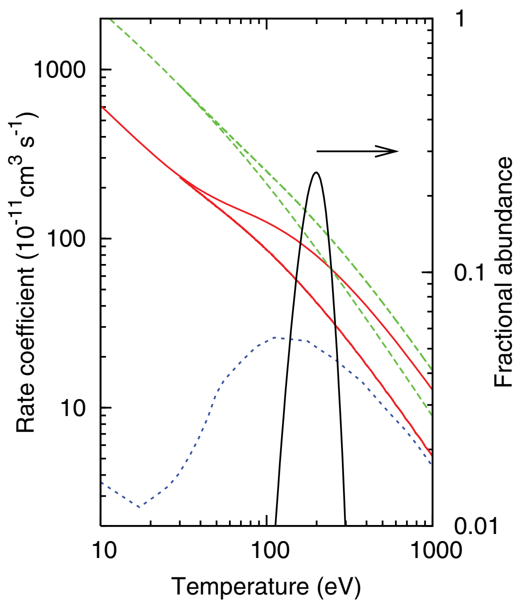

FIG. 8. (Color online) W^{20+} total Maxwellian DR rate coefficients: IC, all resonances and to 140 eV only [solid (red) curves originating on y axis]; experiment [7], to 140 eV and with theory top-up for resonances above 140 eV [long-dashed (green) curves]; and ADAS [31] [short-dashed (blue) curve]. The fractional abundance of W^{20+} in a magnetic fusion plasma is also shown [solid (black) curve originating on x axis].

we add a theoretical top-up (for resonances above 140 eV) to the experimental result, then this difference is reduced to about 40% (at 160 eV) and is 50%–30% over 100–300 eV. The top-up is between 20% and 60% of the experimental result alone over 100–300 eV. The topped-up experimental result is the total (zero-density) DR rate coefficient that we recommend for use in modeling because of the remaining difference between theory and experiment. This difference is attributable to the difference in the contribution from low-energy resonances. The $\Delta n = 0$ resonances as a whole contribute about one-third of the IC total at 160 eV. The factor-of-3-larger experimental contribution from such resonances at low energies means that they contribute significantly more here.

The final results we show in Fig. 8 are those from ADAS [31]. These were determined using the Burgess General Formula (GF) [32]; this is ADAS case A [9], which extends the GF validity to a finite density by the use of a global suppression factor [33]. Those shown here were determined at an electron density close to 0 (10^8 cm^{-3}).

We see that the ADAS [31] results lie between a factor of 10 and a factor of 4.5 below our recommended ones over 100–300 eV. The ADAS results are for dielectronic plus radiative recombination. The radiative contribution dominates in these results below 20 eV because the case A Burgess GF cannot describe the effect of low-lying resonances. Such low-lying resonances can be described by the the BBGP approach [16,17]; this is ADAS case B, which resolves the final recombined state and so is amenable to the collisional-radiative modeling of density effects [34].

The fractional abundance curve we show has been determined using the ADAS case A data at an electron density of 10^{13} cm^{-3}, which is typical of that relevant to magnetic fusion edge plasmas [1]. It differs slightly from the one shown by Schippers *et al.* [7], which is due to Pütterich [35] and at 10^{14} cm^{-3}. It is appropriate to use a finite-density abundance to indicate the plasma relevant temperatures on which to focus our comparisons of zero-density rate coefficients because the temperature of peak abundance is density sensitive. The use of rate coefficients which are up to a factor of 10 larger, though, is likely to move the peak abundance to a higher temperature. (Similar increases in the DR rates to be used can be expected for adjacent ionization stages.)

1. Density effects

A rigorous treatment of density effects on DR rate coefficients and their consequential effect on the ionization balance of W^{20+} and adjacent ionization stages is beyond the scope of the present work. We can make some observations, though. The ADAS rate coefficient is reduced by a factor of 2 at an electron density of 10^{13} cm^{-3} (not shown) compared to that at zero density. This is due to the stepwise ionization of high-n ($\gtrsim$10) Rydberg states following recombination. The new recommended total DR rate coefficients contain a large contribution from low-energy resonances of low n ($\lesssim$10). If we assume that the high-n contributions to both are broadly similar, then we can expect maybe a 10%–20% reduction in the new recommended values over 100–300 eV. Similar (reduced) effects can be expected for adjacent ionization stages. This means that the corresponding fractional abundances are likewise less sensitive to the electron density than indicated by the current ADAS data. A revision

TABLE I. Recommended total (zero-density) dielectronic recombination rate coefficient fitting coefficients c_i (cm^3 s^{-1} [eV]$^{3/2}$) and E_i (eV) for the initial ground level of W^{20+}.

i	c_i	E_i
1	4.025(−7)[a]	1.093(+0)
2	7.697(−7)	9.153(+0)
3	1.065(−6)	3.425(+1)
4	1.487(−6)	1.205(+2)
5	2.177(−6)	2.384(+2)

[a] (m) denotes $\times 10^m$.

of the density-dependent ionization balance of f-shell tungsten ions is clearly needed.

2. Fitting coefficients

It is often convenient for simple modeling purposes to fit the total Maxwellian DR rate coefficient (α) to the functional form

$$\alpha(T) = T^{-3/2} \sum_i c_i \exp\left(\frac{-E_i}{T}\right),$$

where the E_i are in the units of temperature T (e.g., eV) and the units of c_i are then cm^3 s^{-1} [eV]$^{3/2}$.

In Table I we present these fitting coefficients for the recommended (experiment topped-up by theory) total zero-density DR rate coefficient for the initial ground level of W^{20+}. The fit is accurate to better (often much better) than 1% over 1–1000 eV.

The total DR rate coefficient can be taken to be the total recombination rate coefficient. The contribution from radiative recombination is negligible over the given temperature range, as is that from three-body recombination at the densities of interest to magnetic fusion plasmas.

V. CONCLUSION

We have calculated IC DR rate coefficients for W^{20+} which include all significant one-electron promotions plus capture. A factor of 3 difference from experiment remains at low energies. We have demonstrated that this can be removed if we assume complete chaotic mixing of multiply excited near-threshold configurations. A similar finding was obtained by Flambaum *et al.* [15] for Au^{25+}. The difference between theory and (topped-up) experiment at energies relevant to magnetic fusion modeling for ITER is somewhat less, *viz.*, between a factor of 2 and a factor of 1.5 over 100–300 eV. The DR data used by ADAS for such modeling needs to be updated since the current Burgess GF case A results lie between a factor of 10 and a factor of 4.5 below our new recommended values over 100–300 eV. Our CA, LS-coupling, and IC results are all in close accord (20%) above 100 eV, which suggests that DR rate coefficients for complex W ions can be determined readily to within a factor of 2 for modeling purposes. Similar behavior can be expected for related complex ions of other heavy elements. Determination of such DR rate coefficients which are accurate to the ~20% level remains problematic, however.

Note added. Recently we became aware of a preprint [36] which considers the near-threshold recombination of W^{q+} (q = 18–25).

ACKNOWLEDGMENTS

We would like to thank Stefan Schippers for providing the experimental data in numerical form. One of us (N.R.B.) would like to thank Gleb Gribakin for clarifying the methodology used in Ref. [15]. This work was supported in part by a Euratom Framework 7 Support Action Agreement with the University of Strathclyde and US Department of Energy grants to Auburn University.

[1] T. Pütterich, R. Neu, R. Dux, A. D. Whiteford, M. G. O'Mullane, and the ASDEX Upgrade Team, Plasma Phys. Control. Fusion **50**, 085016 (2008).
[2] [http://www.iter.org].
[3] ITER Physics Basis, Nucl. Fusion **39**, 2137 (1999).
[4] R. Aymar, P. Barabaschi, and Y. Shimomura (for the ITER Team), Plasma Phys. Control. Fusion **44**, 519 (2002).
[5] [http://en.wikipedia.org/wiki/Cadarache].
[6] [http://www.efda.org/jet/].
[7] S. Schippers, D. Bernhardt, A. Müller, C. Krantz, M. Grieser, R. Repnow, A. Wolf, M. Lestinsky, M. Hahn, O. Novotný, and D. W. Savin, Phys. Rev. A **83**, 012711 (2011).
[8] S. Schippers, D. Bernhardt, M. Grieser, M. Hahn, C. Krantz, M. Lestinsky, O. Novotný, R. Repnow, D. W. Savin, A. Wolf, and A. Müller, Phys. Scripta T **144**, 014039 (2011).
[9] H. P. Summers, *The ADAS User Manual, v2.6* (2004); [http://www.adas.ac.uk].
[10] C. Z. Dong, private communication (2011).
[11] M. F. Gu, Can. J. Phys. **86**, 675 (2008).
[12] C. P. Ballance, D. C. Griffin, S. D. Loch, and N. R. Badnell, J. Phys. B **45**, 045001 (2012).
[13] N. R. Badnell, Comp. Phys. Commun. **182**, 1528 (2011).
[14] G. F. Gribakin, A. A. Gribakina, and V. V. Flambaum, Aust. J. Phys. **52**, 443 (1999).
[15] V. V. Flambaum, A. A. Gribakina, G. F. Gribakin, and C. Harabati, Phys. Rev. A **66**, 012713 (2002).
[16] A. Burgess, Astrophys. J. **139**, 776 (1964).
[17] N. R. Badnell, M. O'Mullane, H. P. Summers, Z. Altun, M. A. Bautista, J. Colgan, T. W. Gorczyca, D. M. Mitnik, M. S. Pindzola, and O. Zatsarinny, Astron. Astrophys. **406**, 1151 (2003).
[18] N. R. Badnell and M. S. Pindzola, Phys. Rev. A **39**, 1685 (1989).
[19] V. V. Flambaum, A. A. Gribakina, G. F. Gribakin, and M. G. Kozlov, Phys. Rev. A **50**, 267 (1994).
[20] A. Hoffknecht, O. Uwira, S. Schennach, A. Frank, J. Haselbauer, W. Spies, N. Angert, P. H. Mokler, R. Becker, M. Kleinod, S. Schippers, and A. Müller, J. Phys. B **31**, 2415 (1998).
[21] N. R. Badnell, J. Phys. B **39**, 4825 (2006).

[22] N. R. Badnell, A. Foster, D. C. Griffin, D. Kilbane, M. O'Mullane, and H. P. Summers, J. Phys. B **44**, 135201 (2011).
[23] M. S. Pindzola, D. C. Griffin, and C. Bottcher, *Atomic Processes in Electron–Ion and Ion–Ion Collisions*, *NATO ASI B*, Vol. 145, edited by F. Brouilliard (NATO, Brussels, 1986), p. 75.
[24] D. C. Griffin, M. S. Pindzola, and C. Bottcher, Phys. Rev. A **31**, 568 (1985).
[25] C. P. Ballance, S. D. Loch, M. S. Pindzola, and D. C. Griffin, J. Phys. B **43**, 205201 (2010).
[26] R. D. Cowan, *The Theory of Atomic Structure and Spectra* (University of California Press, Berkeley, 1981).
[27] R. D. Cowan and D. C. Griffin, J. Opt. Soc. Am. **66**, 1010 (1975).
[28] E. U. Condon and G. H. Shortley, *The Theory of Atomic Spectra* (Cambridge University Press, Cambridge, 1935).
[29] G. F. Gribakin and S. Sahoo, J. Phys. B **36**, 3349 (2003).
[30] G. Gwinner, A. Hoffknecht, T. Bartsch, M. Beutelspacher, N. Eklöw, P. Glans, M. Grieser, S. Kröhn, E. Lindroth, A. Müller, A. A. Saghiri, S. Schippers, U. Schramm, D. Schwalm, M. Tokman, G. Wissler, and A. Wolf, Phys. Rev. Lett. **84**, 4822 (2000).
[31] A. Foster, Ph.D. thesis, University of Strathclyde, Glasgow, UK (2008).
[32] A. Burgess, Astrophys. J. **141**, 1588 (1965); A. Burgess and A. S. Tworkowski, *ibid.* **205**, L105 (1976); A. L. Merts, R. D. Cowan, and N. H. Magee Jr., Los Alamos Scientific Laboratory Report LA-6220-MS (1976).
[33] A. Burgess, Smithsonian Ap. Obs. Rep. **174**, 47 (1965) and unpublished; B. W. Shore, Lawrence Livermore Laboratory Report UCIR-854 (1975).
[34] A. Burgess and H. P. Summers, Astrophys. J. **157**, 1007 (1969).
[35] T. Pütterich, Ph.D. thesis, University of Augsburg, Augsburg, Germany (2005).
[36] V. A. Dzuba, V. V. Flambaum, G. F. Gribakin, and C. Harabati, e-print arXiv:1204.3707v1 [physics.atom-ph].